Article:

Bahar Hooshdaran, Masoud Haghshenasfard, Seyyed Hossein Hosseini, Mohsen Nasr Esfahany, Gartzen Lopez, Martin Olazar. CFD modeling and experimental validation of biomass fast pyrolysis in a conical spouted bed reactor. Journal of Analytical and Applied Pyrolysis 154 : (2021) // Article ID 105011

Received 28 August 2020, Revised 13 October 2020, Accepted 23 December 2020, Available online 30 December 2020.

https://doi.org/10.1016/j.jaap.2020.105011

CFD modeling and experimental validation of biomass fast pyrolysis in a conical spouted bed reactor

Bahar Hooshdaran[a], Masoud Haghshenasfard[a*], Seyyed Hossein Hosseini[b], Mohsen Nasr Esfahany[a], Gartzen Lopez[c,d], Martin Olazar[c]

[a] Department of Chemical Engineering, Isfahan University of Technology, Isfahan 84156-83111, Iran

[b] Department of Chemical Engineering, Ilam University, 69315-516 Ilam, Iran

[c] Department of Chemical Engineering, University of the Basque Country UPV/EHU, Bilbao, Spain

[d] IKERBASQUE, Basque Foundation for Science, Bilbao, Spain

*Corresponding author: Masoud Haghshenasfard, Email: haghshenas@iut.ac.ir

Abstract

A 2D Euler-Euler multiphase computational fluid dynamics (CFD) model in conjunction with the kinetic theory of granular flow (KTGF) was applied to describe the biomass pyrolysis in a spouted bed reactor. The primary interest in this work was the development of a CFD hydrodynamic model of the reactor coupled with a pyrolysis kinetic model for the prediction of biomass pyrolysis product yields (gas, bio-oil, and char). The kinetic model is based on three parallel reactions for the formation of the pyrolysis products and a secondary reaction of gas formation from bio-oil. The CFD hydrodynamic model suitably predicts the behavior of the spouting regime, and its simultaneous resolution with the kinetic model leads to a satisfactory quantitative agreement between the predicted and experimental values for bio-oil and gas yields. This study is evidence of the great potential of CFD techniques for the design, optimization, and scale-up of conical spouted bed reactors.

Keywords

Computational fluid dynamics (CFD); bio-oil; fast pyrolysis; spouted bed reactor

1. Introduction

There is now an increasing concern for the environment, especially in developed countries. This is boosting the replacement of fossil fuels with biofuels to reduce greenhouse gas emissions. According to the Paris Climate Agreement approved in November 2016, countries must keep the increase in the global average temperature to well below 2℃ above pre-industrial levels, and pursue efforts to limit the increase to 1.5℃, since this would significantly reduce the risks and impacts of climate changes [1].

Biomass is known as the most abundant source of renewable energy, as it is available in all countries in various forms, and can be converted into useful forms of energy using different thermochemical conversion techniques. The utilization of the energy derived from biomass feedstocks can lead to a decrease in current environmental problems, such as CO_2 and SO_2 emissions into the atmosphere [2]. Biomass wastes can be turned into clean and renewable energy by many conversion processes. Among the different thermochemical conversion processes, pyrolysis is a promising one that can produce gases, liquids, and solids, which takes place in the absence of oxygen or air [3].

The main products of biomass pyrolysis are usually known as condensable and non-condensable volatiles and char. The condensable volatile fraction is often called bio-oil, and the non-condensable gases are composed of mainly CO, CO_2, H_2, and C_1-C_2 hydrocarbons [4,5]. Bio-oil is the main product fraction of the biomass fast pyrolysis process; it has lower nitrogen and sulfur content in comparison to fossil fuels and can be used as an alternative fuel in turbines and diesel engines [5,6]. However, the bio-oil must be upgraded to be

applicable in power plants and diesel engines [7-9]. Moreover, several researchers have investigated different upgrading methods to stabilize and deoxygenate the bio-oil [10,11].

One of the most abundant biomass types in the world, especially the Basque region, is the pinewood (*pinus insignis*) straws taken from pine trees. The radiata pine (*pinus insignis*) forests have been created in most parts of the world because of the demand for various woody products. These trees can be adapted to different climatic conditions and are mostly planted in Australia, Chile, New Zealand, Spain, and South Africa [12]. According to statistics, 271 million ha of planted forests exist globally, of which 141 million ha are known as wood farms [13]. There is 4.2 million ha of radiata pine plantations that involve a small part of the total planted forests. However, these coniferous plants are widely cultivated as they are so productive and have many applications in woody products. In Spain, the radiata pine trees occupy about 287 000 ha, mainly located in the Basque region. The 226 000 ha of such trees are in certain areas (pure stands) [14]. The annual sawlogs derived from these trees are 1.5 million m^3 consisting of 20 percent of the Spanish conifer cut.

It is to note that the pyrolysis process applied to pinewood straws can lead to high bio-oil and gas yield due to its high volatile matter, carbon, and oxygen contents, being 73.4, 49.33, and 44.57 wt %, respectively [15]. Therefore, examining an appropriate kinetic model of such biomass type is necessary in order to design and scaling-up the pyrolysis reactor.

Several models have been developed for understanding devolatilization during biomass pyrolysis processes [16-18]. These models could satisfactorily predict product distributions at various temperatures and residence times in the pyrolysis processes. So far, the Computational Fluid Dynamic (CFD) method has been recognized as a useful tool in predicting the product yields of chemical processes, as well as plant design and optimization. Most of the recent CFD studies were applied to biomass pyrolysis in fluidized bed reactors

[19-23]. Papadikis et al. [24-29] simulated biomass fast pyrolysis in fluidized beds assuming two Eulerian phases and one Lagrangian phase in a 3-D domain. They examined the effect of sphericity and particle size on char entrainment, heat, momentum, and mass transfer in a bubbling fluidized bed, as well as the impact of particle size on the heat transfer coefficient. The geometrical optimization of the bubbling fluidized bed has also been approached based on CFD, which allowed improving the performance of the reactor and quality of the fluidization by avoiding stationary bubbles. Boateng and Mtui [30] used a 2-D domain in a similar approach. In another study by Xue and co-workers [31,32], three Eulerian phases were evaluated in a 2-D domain and another in a 3-D domain, and a good agreement between simulation and experimental results was attained. Mellin and co-workers [33] chose a two-phase Eulerian approach for fast biomass pyrolysis in a fluidized bed to predict the product distribution and vapor phase dynamics in a 3-D domain. Model predictions and experimental results were compared, and a good agreement was obtained for product yields.

Conical spouted bed reactors perform even better than conventional fluidized beds in the pyrolysis of various wastes since the vigorous circulation of the solid particles allows employing particles coarser than those used in fluidized beds (with an average diameter of 1 mm or well above), which also promotes heat and mass transfer between phases [34]. Moreover, smaller particles can be handled by draft tubes utilization, and the energy required for opening the spout may be significantly decreased below that required in plain conical spouted beds. Furthermore, draft tubes also allow reducing bed pressure drop [35,36]. Accordingly, the conical spouted bed reactor (CSBR) technology is far more cost-effective in comparison with conventional fluidized beds and has attracted the attention of many researchers. Therefore, this technology has been utilized as an alternative to fluidized beds

in several processes requiring vigorous particle motion, such as drying, coating, gasification, pyrolysis, and so on [37-47].

As mentioned earlier, most CFD studies focused on modeling and optimizing biomass pyrolysis processes in fluidized beds. Besides, these studies have investigated the impact of different operating conditions, such as biomass particle size, sphericity, superficial gas velocity, operating temperature, and different biomass feedstocks on the product yields [19,27,29,48]. The effect geometrical parameters have on the spouted bed hydrodynamics has been extensively investigated by CFD [37,42,49], but its impact on pyrolysis product yields has not yet been studied.

The aim of this study is to propose a model for predicting the evolution of biomass pyrolysis products in a draft tube conical spouted bed reactor based on the Eulerian two-phase flow approach. This approach is especially suitable to study in detail the interaction between sand and biomass mixture with the gas phase, as well as the gas and solid flow patterns in the reactor. Moreover, the kinetic model applied in this simulation considers secondary reactions in the gas phase, with these reactions depending on gas residence time. The kinetic parameters of this model were determined in the previous study by fitting the experimental results obtained in a wide range of temperatures and residence times [15]. It should be noted that the reactor design plays a crucial role in the hydrodynamic stability and product formation in the biomass pyrolysis [50, 51].

Although the overall biomass pyrolysis process includes the complex chemical reactions relating to cellulose, hemicellulose, and lignin decomposition and the formation of a wide variety of oxygenates, it is almost impossible to consider such complicated chemical reactions and numerous reactants and products in a CFD simulation. However, the proposed model must be both accurate and computationally affordable to result in suitable reactor

performance. It is to note that the kinetic reactions used in most CFD modelings of the pyrolysis process are the global kinetic reactions, including a limited number of reactants, products, and reaction steps. Nevertheless, relatively complex reaction kinetics have been employed in several studies [52-57]. The kinetic model used in this study takes into account the most influential parameters affecting the pyrolysis kinetics, i.e., reaction temperature and residence time. The reaction scheme includes the single-step single component decomposition of biomass to gas, bio-oil, and char products.

Moreover, a secondary reaction of the volatiles (bio-oil in the gaseous phase) cracking to produce gases whose extent depends on the residence time has been considered. The kinetic parameters were determined by fitting the experimental results obtained in a bench-scale conical spouted bed reactor in the previous study [15]. The detailed expressions for the kinetic scheme have been described in section 3.

The experimental results obtained in the previous study [15] for the evolution of gas and bio-oil yield with reaction time at different temperatures have been used for validating the simulation approach proposed. It is to note that a CFD simulation model based on the coupling of hydrodynamics with the kinetic model considering the secondary reaction is a tool required for reactor design, simulation, and scale-up.

2. Materials and methods

2.1. Raw material

As mentioned before, the feedstock used in the current study is pinewood (*pinus insignis*), which is one of the most abundant biomass in the region. The HHV, ultimate, and proximate analyses of the biomass have been performed in a Parr 1356 isoperibolic bomb calorimeter, LECO CHNS-932 elemental analyzer, and TGA Q500IR thermogravimetric analyzer,

respectively. The proximate and ultimate analyses of the biomass are summarized in Table 1 [15].

Table 1. Characterization of the biomass used [15].

Ultimate analysis (wt%)	
Carbon	49.33 ± 0.20
Hydrogen	6.06 ± 0.02
Nitrogen	0.04 ± 0.0001
Oxygen	44.57 ± 0.18
Proximate analysis (wt%)	
Volatile matter	73.4 ± 2.0
Fixed carbon	16.7 ± 0.5
Ash	0.5 ± 0.01
Moisture	9.4 ± 0.25
HHV (MJ/kg)	19.8 ± 0.53

2.2. The bench-scale conical spouted bed reactor

The kinetic experiments of the biomass fast pyrolysis were conducted in a bench-scale conical spouted bed reactor at the University of the Basque Country UPV/EHU. A scheme of the reaction unit can be found elsewhere [15]. The plant has been designed for both batch and continuous fast pyrolysis of various biomasses and wastes [58-60]. The dimensions of the reactor used in the simulation are shown in Fig. 1. They are as follows: diameter of the conical section, D_C = 95 mm, the height of the conical section, H_C = 150 mm, inlet diameter, D_0 = 8 mm, length of the draft tube, L_T = 85 mm, draft tube diameter, D_T = 10 mm, and height of the entrainment zone, L_H = 15 mm. A more detailed description of this unit can be found elsewhere [15,60].

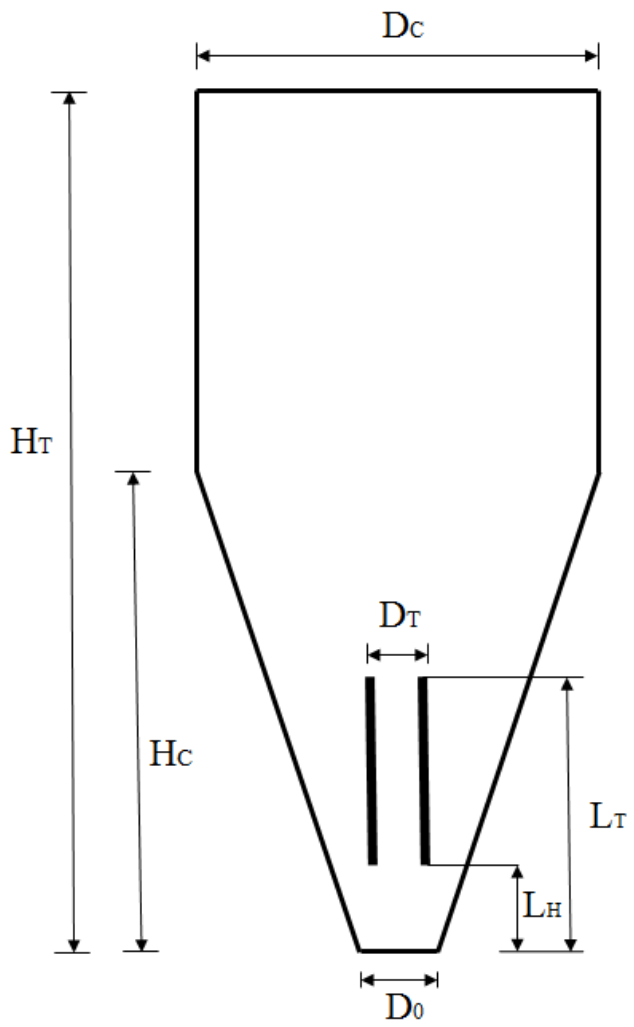

Fig. 1. Dimensions of the CSBR experimental unit used in the simulation.

The spouting gas (Nitrogen) enters at the bottom of the reactor with a constant flow rate and can be controlled by a mass flow meter up to 30 L min^{-1}. The Nitrogen gas flows through a preheater to enter the reactor at the reaction temperature. The bed contains 100 g of sand particles, which are maintained in the bed at isothermal conditions and provide heat to the biomass. The reactor works in discontinuous mode by feeding in each run 1 g of biomass particles with a size of 1-2 mm from the top of the reactor. Samples of the volatile stream (bio-oil in the gaseous phase and non-condensable gases) have been taken at specific

operating times and injected into a GC (Agilent 6890) and a micro GC (Varian 4900), which are connected in-line to the bench-scale plant, to determine gas and liquid yields. The reactor walls are heated by an electrical heater whose temperature can be set for each experiment. A thermocouple is placed in the bed to control the temperature and maintain the bed at isothermal conditions. Runs have been performed at three different temperatures of 450, 500, and 550 ºC to investigate the impact of temperature on product yields. Furthermore, each run has been repeated three times to obtain precise results. The runs lasted until no volatiles were formed in the process, and the reaction finished, which occurred at 300, 200, and 120 s, for 450, 500, and 550 ºC pyrolysis temperatures, respectively [15].

The effect of residence time on the pyrolysis process has also been studied using three different sand particle sizes of 0.1-0.2 mm, 0.4-0.6 mm, and 1-2 mm, which required nitrogen flow rates of 2, 6, and 11 L min^{-1}, respectively. As described in the previous work [15], the sand particle size modification allowed for examining the impact of residence time on the secondary reaction as long as the change in sand particle size gave way to modifying gas flow rate. It is to note that the ratio between the operating and the minimum spouting velocity must be maintained at u/ums=1.5 to obtain a similar spouting regime in all cases and ensure a suitable comparison of the obtained results. Hence the nitrogen flow rate must be changed for each particle size, allowing comparable heat transfer rate between the sand and biomass particles as long as a similar solid circulation rate is attained. However, the biomass particle size does not change in all cases because it does not affect the reactor hydrodynamics significantly (1 gram in each experiment). In the same line, the biomass/sand rate is not a relevant parameter under the studied conditions. The mass of biomass per run was selected as it ensures a suitable analysis of pyrolysis products using GC and micro GC techniques. It is noteworthy that selecting such sand particle sizes allows performing the experiments with

minimum impact on heat transfer rate and bed behavior as well as maintaining the same ratio between spouting gas velocity and minimum spouting one (u/u_{ms}) in all experiments. It should be noted that heat transfer to an immersed solid in spouted beds mainly depends on the solid circulation rate [34] and this parameter strongly depends on the u/u_{ms} ratio. Therefore, amongst the performed experiments, comparable heat transfer conditions could be expected. The average gas residence times in the bed for the coarse, medium and fine sands have been 0.56, 0.85, and 1.69 s, at 450 °C, 0.53, 0.79, and 1.58 s at 500 °C and 0.50, 0.74, and 1.49 s at 550 °C.

In the current simulation, the medium particle size of 0.4-0.6 mm, which had a slight variation in residence time, with the nitrogen flow rate of 6 L min^{-1} has been used at the three studied temperatures. The sand bulk and real densities are 1280 kg m^{-3} and 2600 kg m^{-3}, respectively. Moreover, the residence time downstream of the reactor was not considered due to its limited potential impact on the results. This is also explained in section 4.1, with more details.

3. Model description

The commercial CFD package ANSYS FLUENT version 18 was used to study the hydrodynamic parameters and predict the reaction rates during the biomass pyrolysis process. The commercial software GAMBIT, version 2.4, has been used to create the geometry and mesh for the plant used in the simulation. Fig 2. illustrates the cross-section of the spouted bed reactor together with the boundary conditions applied in the simulation.

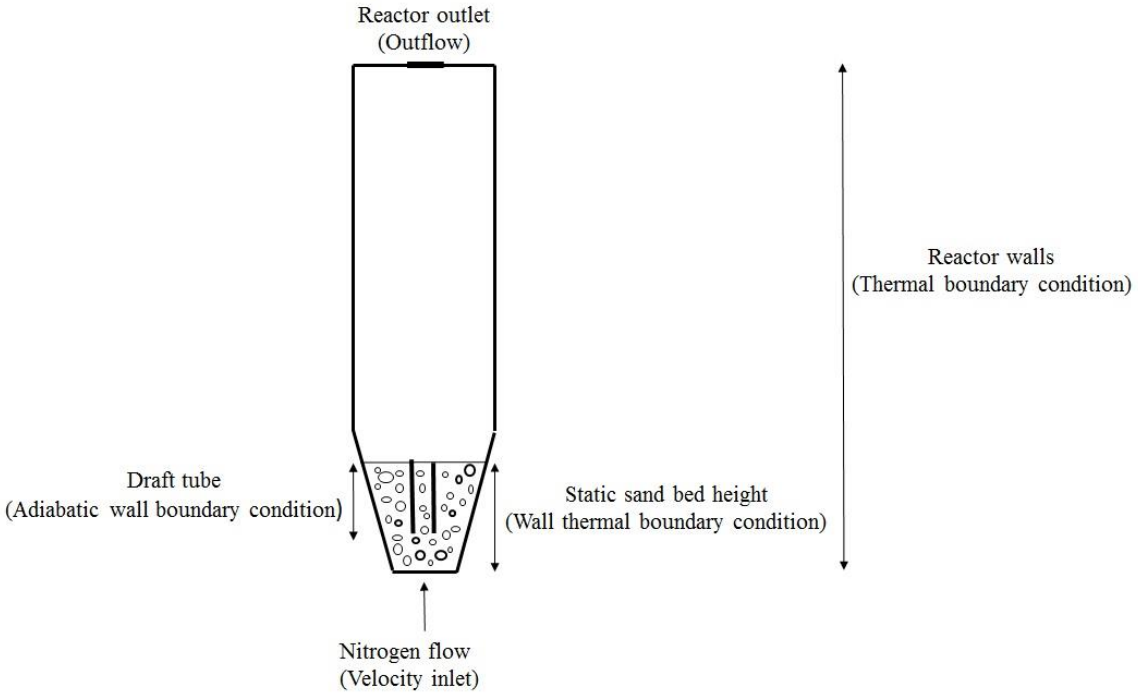

Fig 2. Spouted bed geometry and boundary conditions

In this study, the biomass fraction in the bed is very low compared to that of sand, 0.01; therefore, a simplified approach can be used by assuming only one Eulerian phase for the mixture of sand and biomass particles. This approach has already been examined by Mellin et al. [33] for the continuous pyrolysis of biomass in a fluidized bed. In this procedure, they assumed that the sand particles influence the fluid phase, and the impact of biomass particles on the hydrodynamics of the bed is insignificant. This approach successfully predicts the products of the fast pyrosis process. The kinetic model used in the current simulation consists of three parallel, single-component, first order, and homogenous reactions for the formation of bio-oil, gas, and char from biomass, Fig. 3. Moreover, a secondary cracking reaction of bio-oil to produce gases has also been considered, Fig. 3. It is to note that this reaction rate

is proportional to the bio-oil concentration and consequently depends on the residence time in the reactor, which is of high relevance for scaling up simulations.

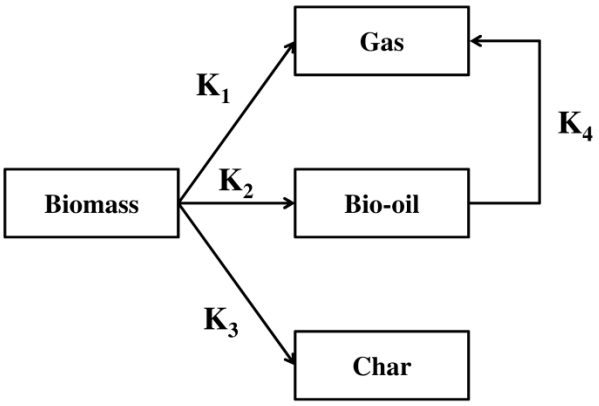

Fig 3. The scheme proposed for the biomass fast pyrolysis reaction.

All reactions have been modeled with the first-order Arrhenius equation, and the kinetic constants of the reactions were determined in the previous study by minimizing the error between the calculated and experimental product formation rates at different temperatures [15]. As mentioned in the introduction section, several kinetic models have been employed in CFD modeling of biomass pyrolysis processes [52-57]. These models are the first-order reactions whose kinetic constants follow the Arrhenius equation. Although the actual lignocellulosic biomass pyrolysis mechanism is complex and not known completely, the first-order kinetic models suitably predict the product formation rates. This is also the case of the model used in this study. In fact, the model can predict not only the effect of temperature but also that of residence time in the reactor, which is essential for its use in the reactor scale-up and simulation. Table 2 shows the frequency factor and activation energy used in the model for each reaction considered in this study. It should be remarked that the kinetic model obtained faithfully predicts the experimental results for different temperatures and residence times, which guarantees its applicability in a wide range of process conditions.

Table 2. Kinetic constants used in the simulation for the biomass pyrolysis reaction [15].

Reaction	k^0 (s^{-1})	E (kJ mol^{-1})
1. Biomass ⟶ Gas	536.2	76.8
2. Biomass ⟶ Bio − oil	4.3	33.4
3. Biomass ⟶ Char	1.2 10^{-2}	5.6
4. Bio − oil ⟶ Gas	138.3	55.6

As mentioned above, the Euler-Euler multiphase model is applied in the current simulation. In the Eulerian framework, the gas and solid phases are considered as inter-penetrating continua. The primary phase is the nitrogen fluid phase, and the solid phase is considered as the secondary and granular phase, which is a mixture of biomass and sand particles. The gas flow (nitrogen and volatile stream) is assumed to be turbulent, and therefore the k-ε standard approach is used, which suitably predicts product formation. Although the value of the Reynolds number at the inlet was 1500, the velocity of the gas stream increased along the draft tube. This accelerated velocity resulted in the formation of eddies on top of the draft tube, leading to Reynolds numbers close to 5000. Such high Reynolds numbers satisfy the assumption of turbulent flow. Fig. 4 shows the velocity vectors of sand and gas stream at t = 30 s and T = 500 °C. As can be seen in Fig. 4b, the typical solid circulation pattern of spouted beds was attained, i.e., the sand particles go upward through the spout region and reach the fountain; then, they descend through the annulus region and go back to the spout region. Fig. 4a displays the big eddies formed on the top of the draft tube, which are created due to the high gas velocity along the draft tube. It is to note that the spouting regime obtained by CFD simulation is similar to that experimentally observed in the laboratory in terms of fountain

height and solid circulation. This result confirms the suitability of this technique for the simulation of hydrodynamics in a conical spouted bed reactor.

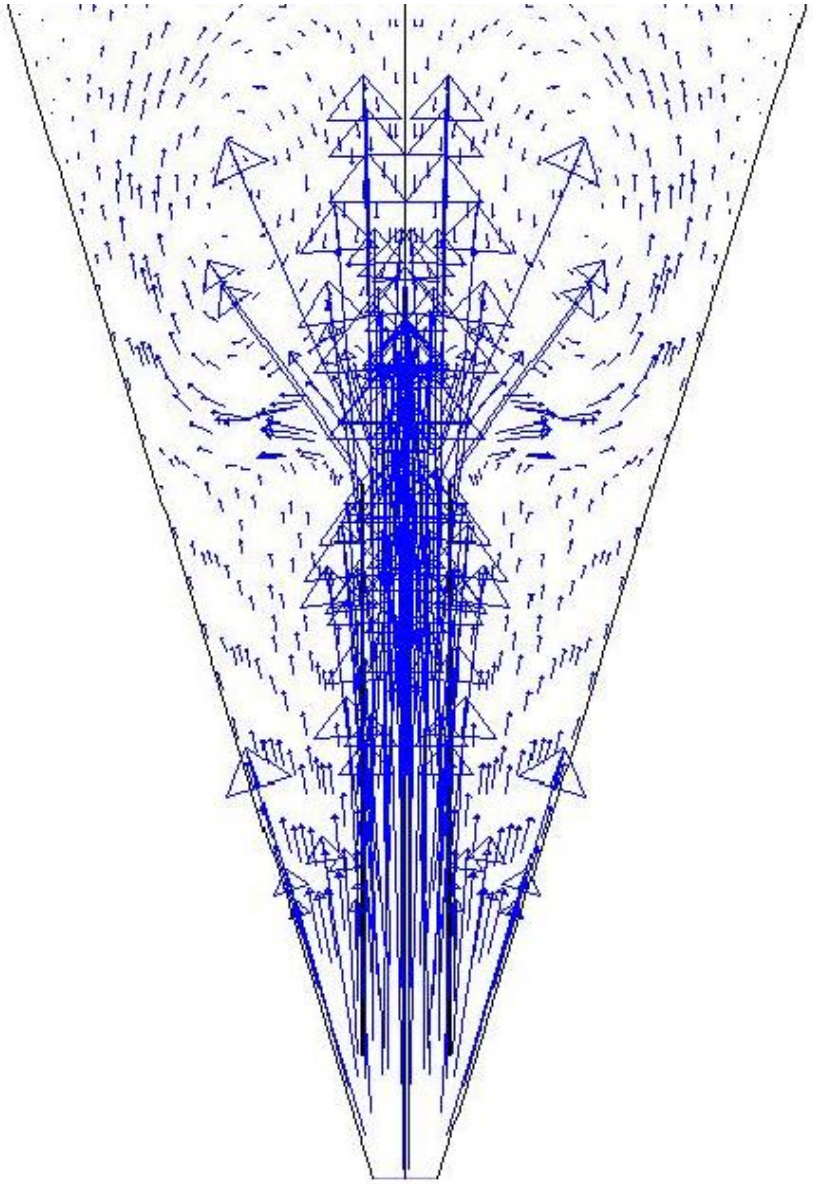

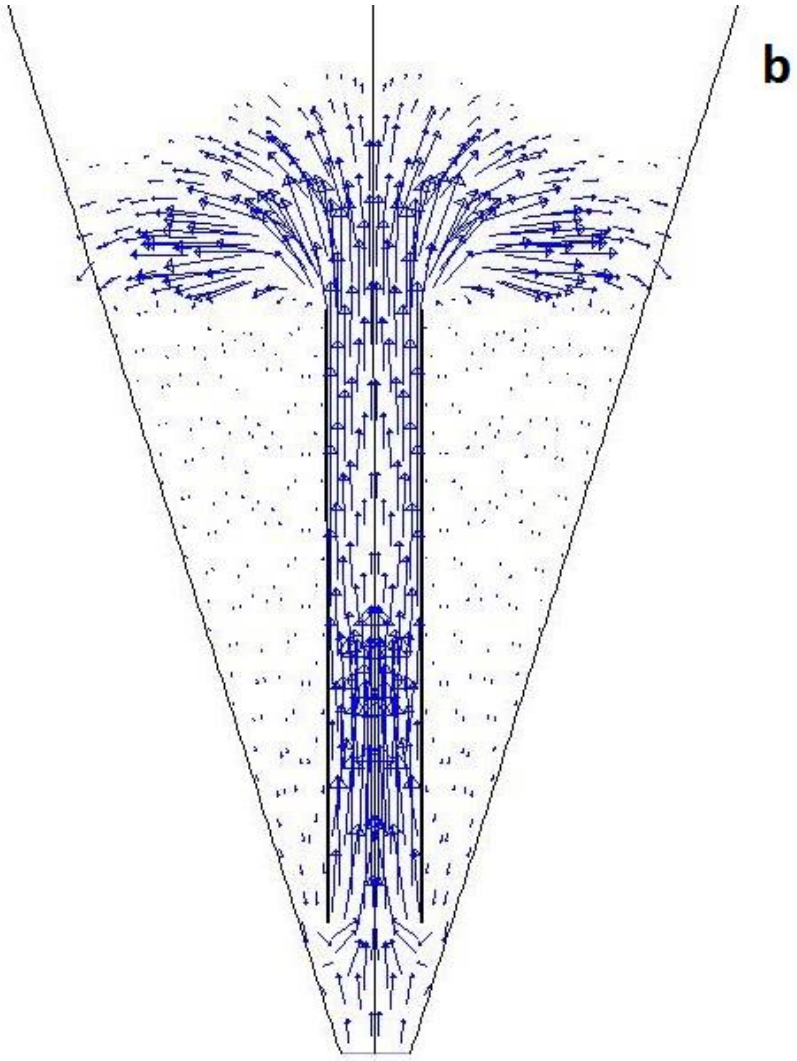

Fig. 4. Velocity vectors of a) gaseous phase and b) sand at t=30 s and T = 500 °C

Following Cammarata et al. [61], a two-dimensional/axisymmetric model was used to reduce the computational time since the phase behavior is symmetric relative to the central axis of the plane, and hence half of the geometry was considered. The pressure-based solver with second-order transient formulation was used, giving rise to the best convergence and prediction of product mass fractions. The time-step size for all models began at 1×10^{-5} s with 100 iterations for each time step. After gradient stabilization, the step size could gradually be increased to 0.0002 s for all models. For all time steps, the maximum value of

the scaled residuals was 1×10^{-3} to ensure convergence between two iterations. The mesh used in the model consisted of 25700 quadrilateral structured cells in a geometry containing grid sizes equal to 8 mm.

A grid independence test was performed to obtain the most appropriate number of grids for saving computational time and attain the best convergence. Fig. 5 displays the time-averaged pressure difference between the inlet and outlet of the reactor to illustrate mesh independence. All the simulation conditions were the same for the five grid sizes, which were performed at T = 500 °C and inlet nitrogen velocity of 2.7 m s^{-1}. Fig. 5 shows that there is no considerable difference between the results of the medium and fine grid. Therefore, the medium mesh (mesh number = 25700) has been preferred to simulate this reactor, which allows obtaining accurate results and saving as much computational time as possible.

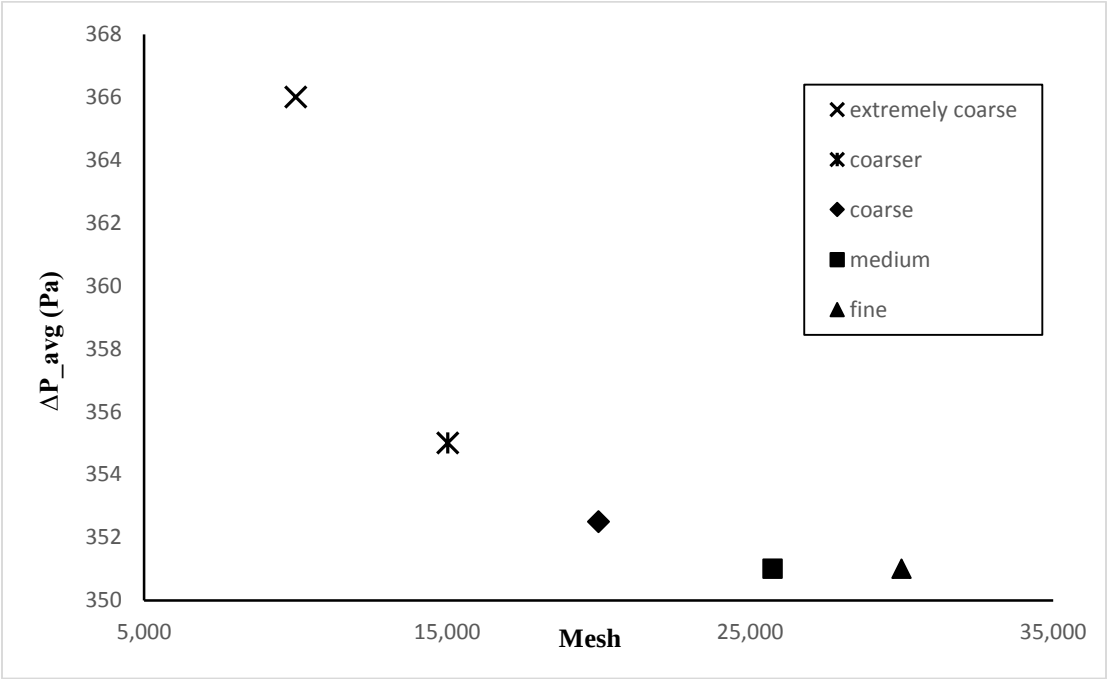

Fig. 5. Mesh independence test for the CFD model.

3.1. Governing equations

The governing equations consist of continuity, momentum, energy, and species transport equations, which are solved by the finite volume method (FVM). These equations are solved for each phase to investigate hydrodynamics, heat transfer, and product formation. As the reactor works in the discontinuous mode in both experimental and simulation studies, the transient forms of the governing equations given below have been used.

Continuity equation for the qth phase

$$\frac{\partial}{\partial t}\left(\alpha_q \rho_q\right) + \nabla.\left(\alpha_q \rho_q \overrightarrow{v_q}\right) = S_q \tag{1}$$

Where α_q represents the volume fraction, ρ_q the density, $\overrightarrow{v_q}$ the velocity and S_q the mass added from the solid phase due to reactions at the gas-solid interphase or any source term defined by the user.

Momentum equation for *the gas phase*

$$\frac{\partial}{\partial t}\left(\alpha_g \rho_g \vec{v}_g\right) + \nabla.\left(\alpha_g \rho_g \vec{v}_g \vec{v}_g\right) = -\alpha_g \nabla p + \nabla.\bar{\bar{\tau}}_g + K_{gs}\left(\vec{v}_s - \vec{v}_g\right) + \alpha_g \rho_g g + \dot{m}_{gs}\vec{v}_g \tag{2}$$

Momentum equation for the solid phase

$$\frac{\partial}{\partial t}\left(\alpha_s \rho_s \vec{v}_s\right) + \nabla.\left(\alpha_s \rho_s \vec{v}_s \vec{v}_s\right) = -\alpha_s \nabla p - \nabla p_s + \nabla.\bar{\bar{\tau}}_s + K_{gs}\left(\vec{v}_g - \vec{v}_s\right) + \alpha_s \rho_s g + \dot{m}_{sg}\vec{v}_s \tag{3}$$

Where $\alpha_s = 1 - \alpha_g$.

Stress tensor equation for the gas phase

$$\bar{\bar{\tau}}_g = \alpha_g \mu_g \left[\left(\nabla \vec{v}_g + \nabla \vec{v}_g{}^T \right) - \frac{2}{3} \nabla . \vec{v}_g \bar{\bar{I}} \right] \quad (4)$$

Stress tensor equation for the solid phase

$$\bar{\bar{\tau}}_s = \alpha_s \mu_s \left[\left(\nabla \vec{v}_s + \nabla \vec{v}_s{}^T \right) + \alpha_s \left(\lambda_s - \frac{2}{3} \mu_s \right) \nabla . \vec{v}_s \bar{\bar{I}} \right] \quad (5)$$

Solid bulk viscosity

$$\lambda_s = \frac{4}{3} \alpha_s \rho_s d_s g_{0,ss} (1 + e_{ss}) \left(\frac{\Theta_s}{\pi} \right)^{1/2} \quad (6)$$

The drag function suggested by Gidaspow [62]

$$K_{gs} = \frac{3}{4} C_D \frac{\alpha_s \alpha_g \rho_g |v_g - v_s|}{d_s} \alpha_g^{-2.65} \text{ for } \alpha_g > 0.8 \text{ (Wen} - \text{Yu drag model)}$$

$$C_D = \begin{cases} \frac{24}{\alpha_g Re_s} \left[1 + 0.15 \left(\alpha_g Re_s \right)^{0.687} \right], & Re_s < 1000 \\ 0.44 & Re_s > 1000 \end{cases} \quad (7)$$

$$K_{gs} = 150 \frac{\alpha_s^2 \mu_g}{\alpha_g d_s^2} + 1.75 \frac{\alpha_s \rho_g |v_g - v_s|}{d_s} \quad \text{for } \alpha_g \leq 0.8 \text{ (Ergun drag model)}$$

Solid shear viscosity

$$\mu_s = \mu_{s,col} + \mu_{s,kin} + \mu_{s,fr} \quad (8)$$

The collisional and kinetic viscosity given by Gidaspow et al. [63]

$$\mu_{s,col} = \frac{4}{5}\alpha_s \rho_s d_s g_{0,ss}(1+e_{ss})\left(\frac{\Theta_s}{\pi}\right)^{1/2} \tag{9}$$

$$\mu_{s,kin} = \frac{10 d_s \rho_s \sqrt{\Theta_s \pi}}{96 \alpha_s g_{0,ss}(1+e_{ss})}\left[1+\frac{4}{5}\alpha_s g_{0,ss}(1+e_{ss})\right]^2 \tag{10}$$

The solid frictional viscosity proposed by Schaeffer [64]

$$\mu_{s,fr} = \frac{P_{s,fr} sin\phi}{2\sqrt{\mathrm{I}_{2D}}} \tag{11}$$

The energy equation for the gas phase

$$\frac{\partial}{\partial t}\left(\alpha_g \rho_g H_g\right) + \nabla.\left(\alpha_g \rho_g Y_g \vec{v}_g H_g\right) = \nabla\left(k_g \nabla T_g\right) + h\left(T_g - T_s\right) + S_g \tag{12}$$

The energy equation for the solid phase

$$\frac{\partial}{\partial t}(\alpha_s \rho_s H_s) + \nabla.(\alpha_s \rho_s Y_s \vec{v}_s H_s) = \nabla(k_s \nabla T_s) + h\left(T_p - T_g\right) + S_s \tag{13}$$

The interphase heat transfer coefficient

$$h = \frac{6 k_g \alpha_s \alpha_g Nu_s}{d_s^2} \tag{14}$$

The solid Nusselt number derived by Gunn [65]

$$\begin{aligned} Nu_s = {} & \left(7 - 10\alpha_g + 5\alpha_g^2\right)\left(1 + 0.7 Re_s^{0.2} Pr^{1/3}\right) \\ & + \left(1.33 - 2.4\alpha_g + 1.2\alpha_g^2\right) Re_s^{0.7} Pr^{1/3} \end{aligned} \tag{15}$$

Species transport equation for the qth phase

$$\frac{\partial}{\partial t}\left(\alpha_q \rho_q Y_i\right) + \nabla.\left(\alpha_q \rho_q Y_i \vec{v}_q\right) = S_q \quad (16)$$

Where Y_i is the mass fraction, and S_q is the reaction source term for each species.

The yields of each pyrolysis component can be calculated as follows:

$$\frac{\partial}{\partial t}(\alpha_{sB}\rho_{sB}Y_B) + \nabla.(\alpha_{sB}\rho_{sB}Y_B\vec{v}_s) = -\rho_{sB}\alpha_{sB}(k_1 + k_2 + k_3)Y_B \quad (17)$$

$$\frac{\partial}{\partial t}\left(\alpha_{gG}\rho_{gG}Y_G\right) + \nabla.\left(\alpha_{gG}Y_G\vec{v}_g\right) = \rho_{sB}\alpha_{sB}k_1Y_B + \rho_{gL}\alpha_{gL}k_4Y_L \quad (18)$$

$$\frac{\partial}{\partial t}\left(\alpha_{gL}\rho_{gL}Y_L\right) + \nabla.\left(\alpha_{gL}Y_L\vec{v}_g\right) = \rho_{sB}\alpha_{sB}k_2Y_B - \rho_{gL}\alpha_{gL}k_4Y_L \quad (19)$$

$$\frac{\partial}{\partial t}(\alpha_{sC}\rho_{sC}Y_C) + \nabla.(\alpha_{sC}\rho_{sC}Y_C\vec{v}_s) = \rho_{sB}\alpha_{sB}k_3Y_B \quad (20)$$

In the equations above, subscripts B, G, L, and C shows biomass, gas, liquid (bio-oil), and char, respectively.

4. Results and discussion

4.1. Model performance and validation

In order to validate the CFD simulation of biomass pyrolysis in a draft tube conical spouted bed reactor, the experimental results obtained in a previous study in a bench-scale unit have been considered. In the experimental work, the evolution of bio-oil and gas yields with reaction time was obtained at the three temperatures of 450, 500, and 550 °C. Furthermore,

the kinetic constants of best fit have been determined by solving the mass balance equations written for different sections of the spouted bed reactor [15].

The yields of bio-oil and non-condensable gases were obtained from the simulation model and compared with the corresponding amounts determined in the experimental work at different reaction times. Char yield could only be measured at the end of each experimental run since it was the non-converted fraction of the biomass, i.e., it could not be monitored and measured throughout the reaction. As mentioned in section 2, the simulations have been done considering a sand particle size of 0.4-0.6 mm and a nitrogen velocity of 2.7 m/s, leading to gas residence times of 0.85, 0.79, and 0.74 s at 450, 500, and 550 °C, respectively.

It should be noted that residence time differs from the reaction time, given that the residence time is referred to the gas gaseous stream average residence time in the reactor, whereas reaction time is the time required for the biomass conversion to products (gas, bio-oil, and char). Furthermore, the residence time is below a second, while the reaction time is over a minute. As mentioned before, secondary reactions in biomass pyrolysis depend on the temperature and residence time of the volatile stream, which enters from the reactor to the condensation section. In fact, a fast quenching of pyrolysis products is usually recommended to hinder secondary reactions and enhance bio-oil yield [66]. In the simulation of biomass pyrolysis, only the reactor volume was considered; however, the auxiliary equipment for gas cleaning and pipes from the reactor to the condenser were not taken into account. It should be pointed out that the experimental unit has a cyclone and a filter located upstream of the condensation unit. However, the temperature in these devices is much lower than that in the reactor, approximately 300 ºC. The extent of secondary reactions can be considered negligible at this moderate temperature in relation to their extent in the pyrolysis reactor; accordingly, the consideration of the simulation approach seems reasonable.

A sample of the sand volume fraction contour at t = 30 s and T = 500 °C is shown in Fig. 6. As observed, the incorporation of a draft tube promoted the development of a stable spouting regime [67-69]. Moreover, the three characteristic regions of spout, annulus, and fountain can be observed clearly with their different voidages.

It is to note that both the spout shape and the fountain height remain unchanged in the temperature range of 450-550 ºC. These findings are consistent with those found by Ye et al. [70], showing that the minimum spouting velocity and hence the spouting regime of the bed do not change significantly in a temperature range of 400-880 ºC for the Geldart B group of particles. Furthermore, the temperature has a positive effect on the hydrodynamic stability of the spouted bed, i.e., after only 0.5 s of simulation, a stable spouting has been established by activating the energy equation for both gas and solid phases in the simulation [70,71].

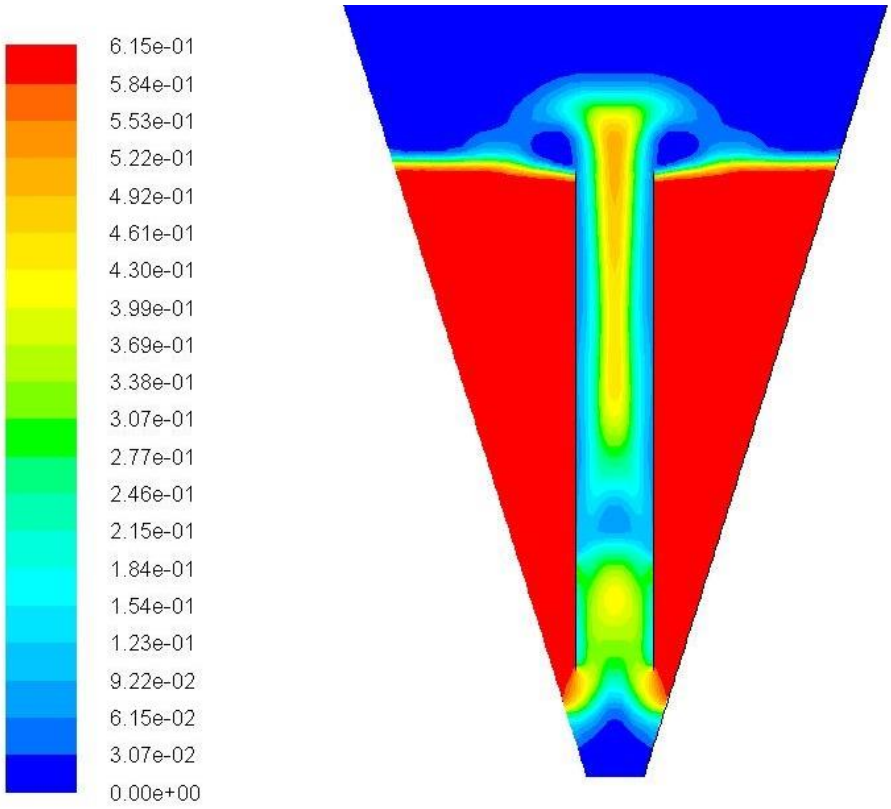

Fig. **6**. Contours of sand volume fraction at 30 s and 500 °C.

Fig. 7 shows a comparison between the simulation results and those of the experiments in terms of the mass (grams) of product fractions formed. Overall, there is a good agreement between experimental data and CFD predictions, with the relative error being in the 10-13% range. At the initial time range of the process, the evolution of product fractions is faithfully predicted by the model, but at the end, the deviations are considerable, i.e., neither the evolution of gas and bio-oil yields in the final time range nor the final gas and bio-oil yields are accurately predicted by CFD simulations. Thus, CFD simulation underestimate the final yields of both gas and bio-oil. Overall, these results are evidence that the simulation model is suitable for predicting product yield evolution in biomass pyrolysis and the influence of temperature on these products in a conical spouted bed reactor. In fact, the impact of temperature on reaction rates was suitably predicted by the CFD model; that is, the time required for biomass conversion was significantly reduced with temperature in both experimental and calculated trends. Moreover, the yield of the gas fraction at high temperatures increases due to the secondary bio-oil cracking reactions considered by the model. The maximum bio-oil yield is achieved at 500 ºC, being consistent with that reported in other fast pyrolysis technologies [66]. However, it can be observed that the CFD results slightly underestimate the experimental yields of both gas and bio-oil for all the studied temperatures. This might be due to the fact that the simulation predicts an incomplete biomass conversion or alternatively, a higher char formation rate than that observed experimentally. These differences could be associated with the deviations in gas and solid residence time distributions in the reactor between experimental conditions and simulated ones. In summary, these results reinforce the validity of this simulation tool for the design and full-scale development of spouted bed reactors for biomass pyrolysis.

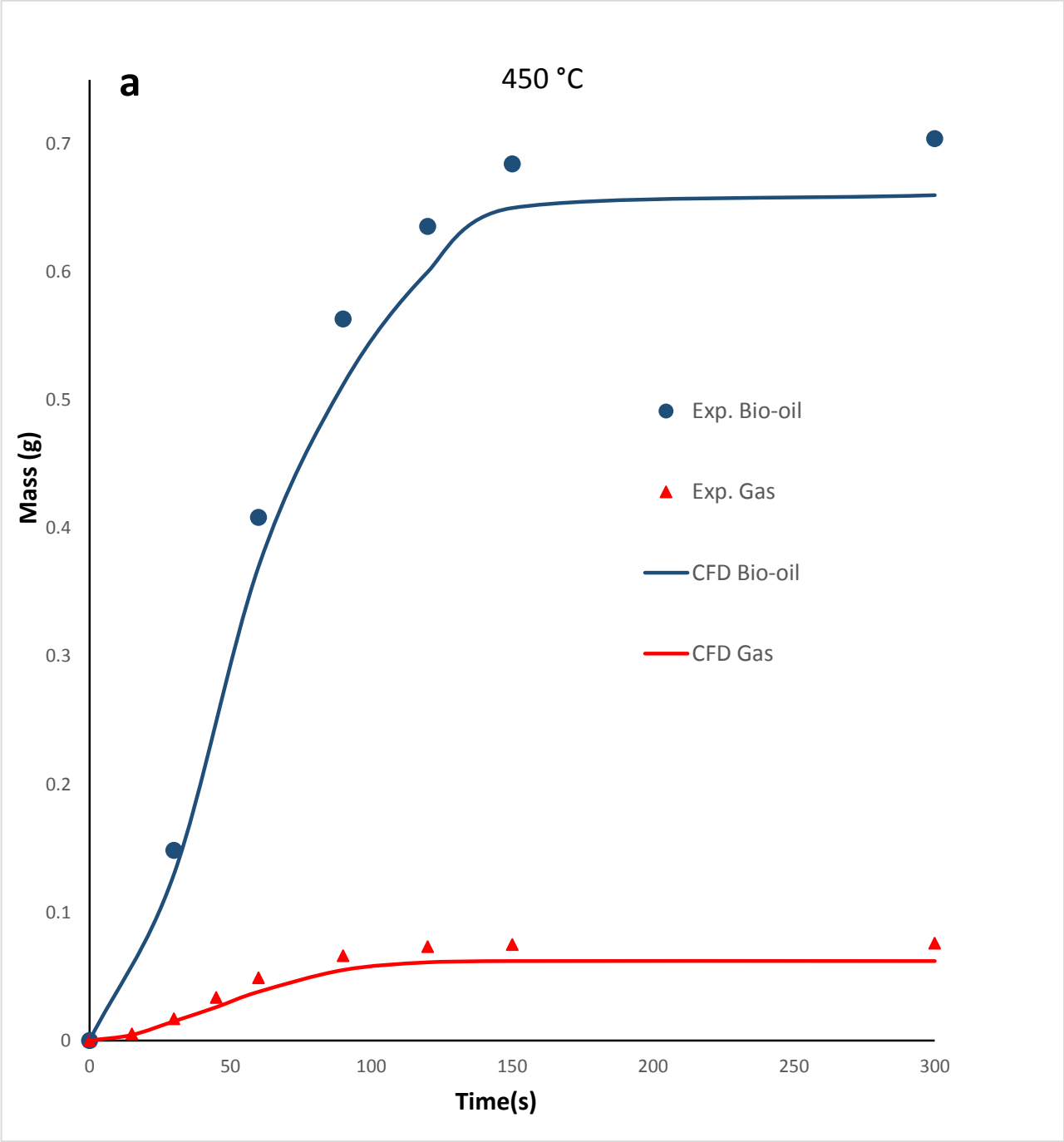
a
450 °C
Mass (g)
0.7
0.6
0.5
0.4
0.3
0.2
0.1
0
0
50
100
150
200
250
300
Time(s)
Exp. Bio-oil
Exp. Gas
CFD Bio-oil
CFD Gas

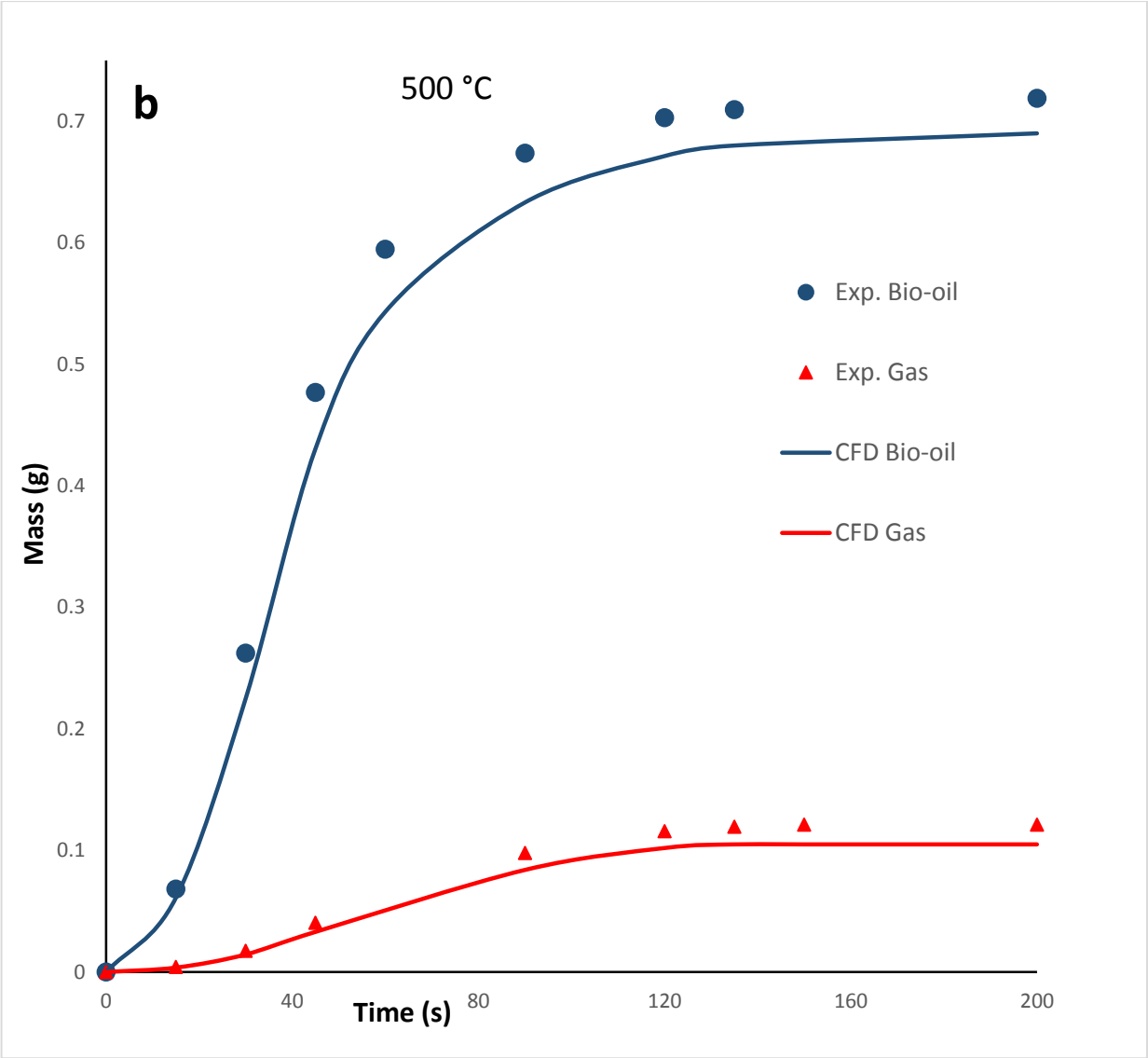
b
500 °C
Mass (g)
Time (s)
0
0.1
0.2
0.3
0.4
0.5
0.6
0.7
0
40
80
120
160
200
Exp. Bio-oil
Exp. Gas
CFD Bio-oil
CFD Gas

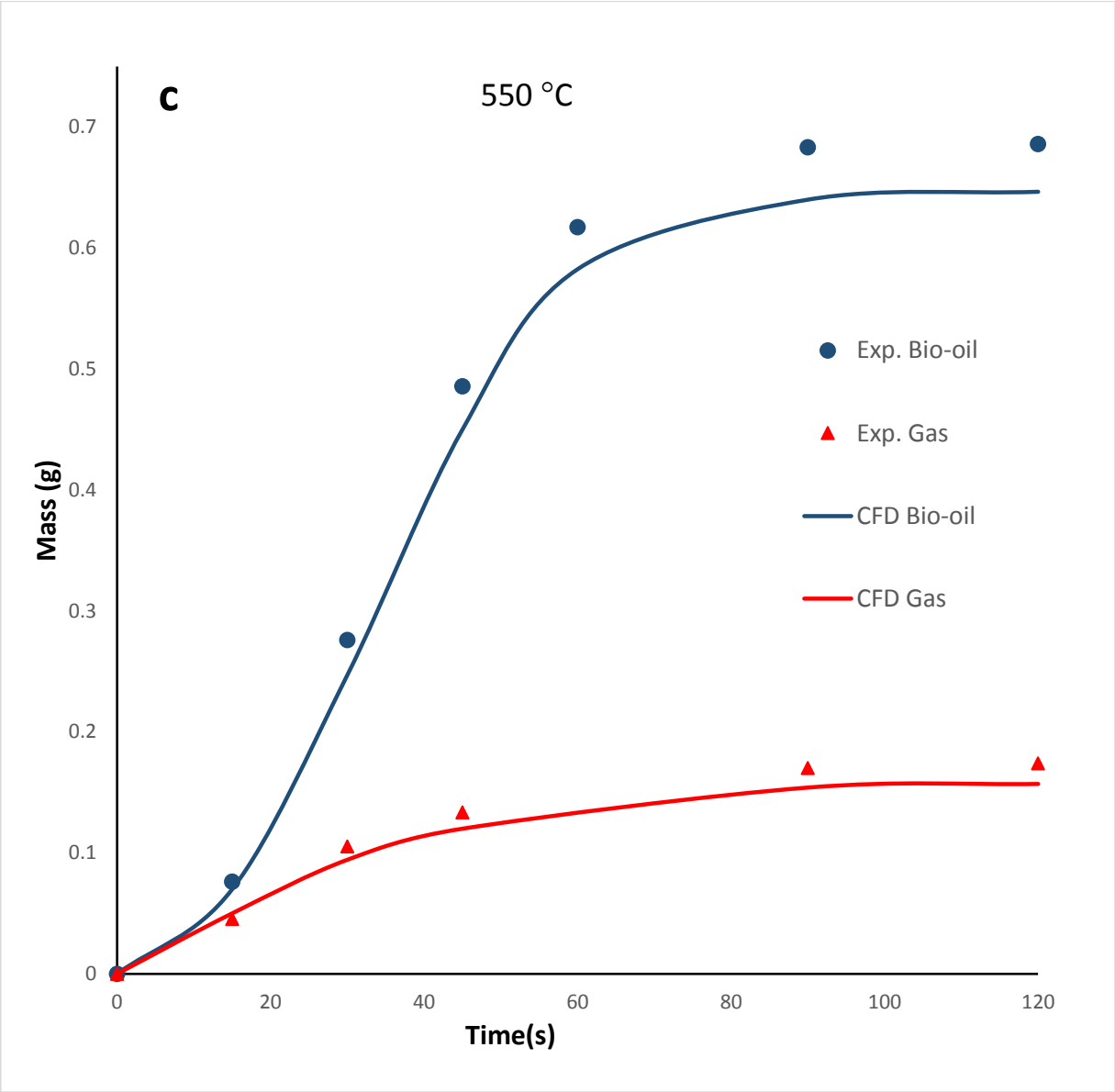

Fig. 7. Validation of the experimental (points) and simulation (lines) results for the evolution of biomass pyrolysis product yields with reaction time at the following temperatures: 450 ºC (7a); 500 ºC (7b), 550 ºC (7c).

4.2. Effect of geometrical parameters on the product values

Once the model has proven to be valid for predicting product formation, it was then used to examine the impact of different geometrical parameters, such as draft tube diameter and height of the entrainment zone, on the evolution of product yields. The entrainment zone height and the draft tube diameter vary from 1 to 2.5 cm and 1 to 1.6 cm, respectively.

Fig. 8. describes the reactor operation in terms of dimensionless design parameters that depicts the bio-oil mass versus the L_H to D_T ratio. It can be concluded that the best reactor design for optimum bio-oil production is at L_H/D_T =1.5, leading to the bio-oil mass equal to 0.061 g.

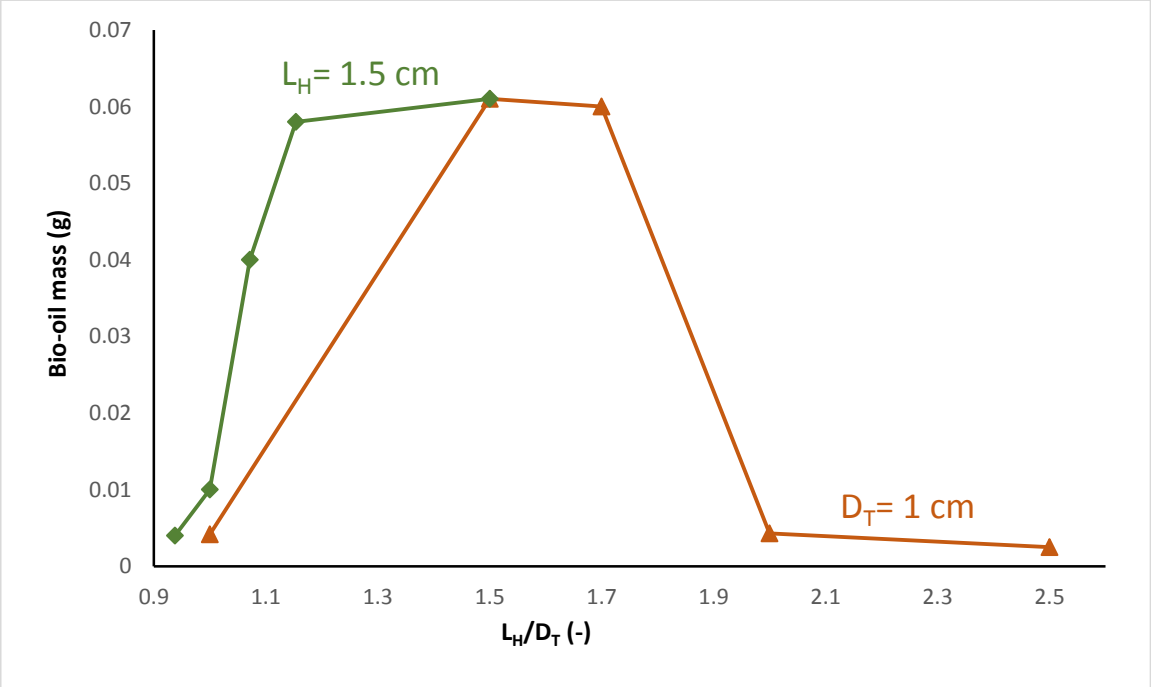

Fig. 8. Effect of L_H/D_T on the bio-oil product at T=500˚C.

The contours of sand volume fraction and nitrogen velocity vectors for L_H/D_T =1.5 and L_H/D_T= 2.5 are displayed in Fig. 9. As can be seen, by increasing the length of the entrainment zone, the bed behavior approaches the spouted bed without draft tube, Fig. 9c (L_H/D_T=2.5), the minimum spouting velocity increases, leading to an increase in the gas velocity [72]. However, increasing the entrainment height causes the spouting regime to be sluggish since

more gas streams divert their path through the annulus resulting in a poor contact of gas and solid particles. On the other hand, the size of the slugs increases with the entrainment height [73], causing a decrease in the production values. The observation of the sluggish spouting by increasing the entrainment height was obtained by different researchers [73,74].

Moreover, due to the long distance between the bottom of the draft tube and the gas inlet, all of the gas streams cannot go upward through the draft tube, the nitrogen velocity decreases on top of the draft tube and hence no eddy form, Fig. 9d. The big eddies formed on both sides of the draft tube for the case L_H/D_T= 1.5 (Fig. 9c) cause a good mixing between phases. From these figures, it can be concluded that the unstable hydrodynamics may lead to low product formation.

It is to note that choosing the draft tube diameters from 1 to 1.6 cm and L_H sizes from 1 to 2.5 cm showed that the spouting regime, together with the biomass pyrolysis products, would be affected significantly by considering the sizes beyond the experimental ones. However, for the case L_H=1 cm and the constant draft tube diameter, the hydrodynamics showed a stable spouting regime, but due to low particle circulation, the product mass fractions were low and demonstrated high deviations from the experimental model. In the model with the draft tube diameter lower than 1 cm (lower than or equal to the gas inlet diameter), the sand particles couldn't go into the tube and hence went upward from the outer sides of the tube. Thereby no spouting regime has been formed. For draft tube diameters of 1.5 cm and 1.6 cm, the hydrodynamics became a little sluggish, and the tube could not increase the nitrogen velocity. Therefore, no eddies formed on top of the draft tube, and the values of the product yields were not as much as the experimental work. Accordingly, for future designs, it is better to consider the draft tube diameters and L_H sizes between 1-1.3 cm and 1.5-1.7 cm, respectively.

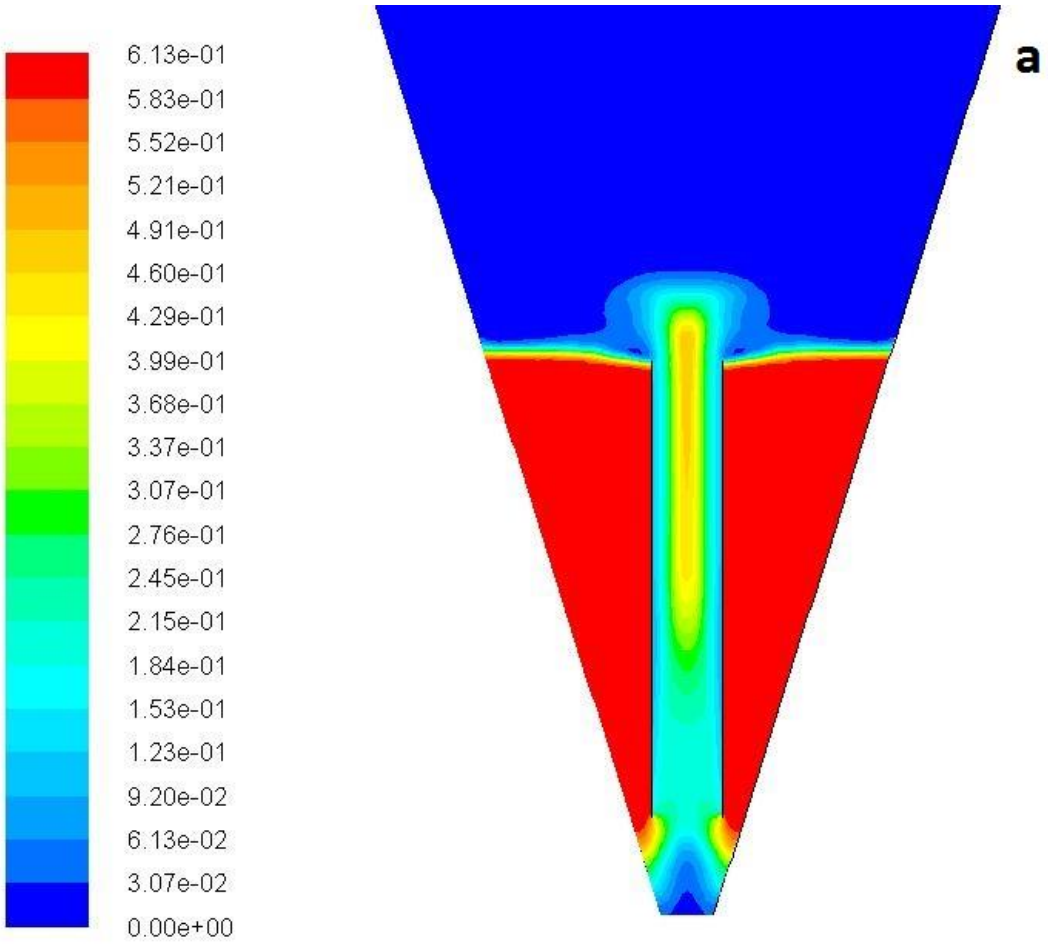
6.13e-01
5.83e-01
5.52e-01
5.21e-01
4.91e-01
4.60e-01
4.29e-01
3.99e-01
3.68e-01
3.37e-01
3.07e-01
2.76e-01
2.45e-01
2.15e-01
1.84e-01
1.53e-01
1.23e-01
9.20e-02
6.13e-02
3.07e-02
0.00e+00
a

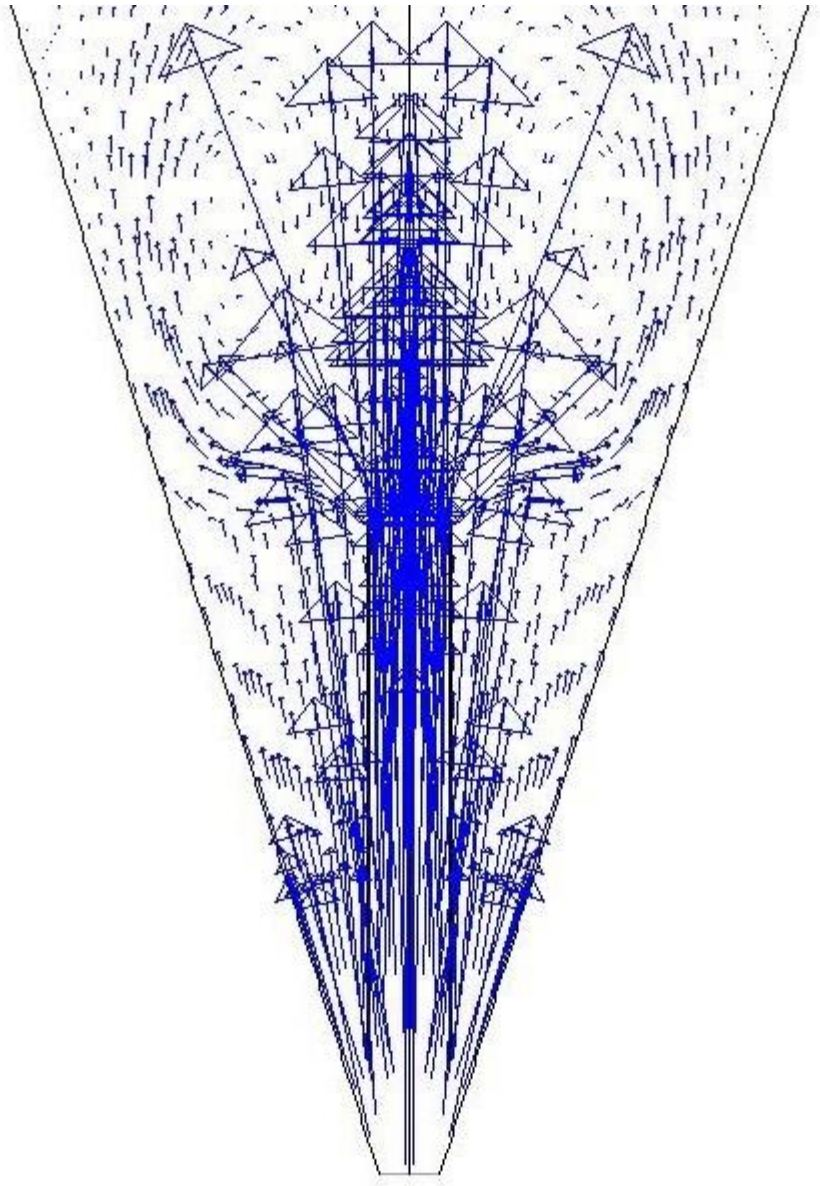
b

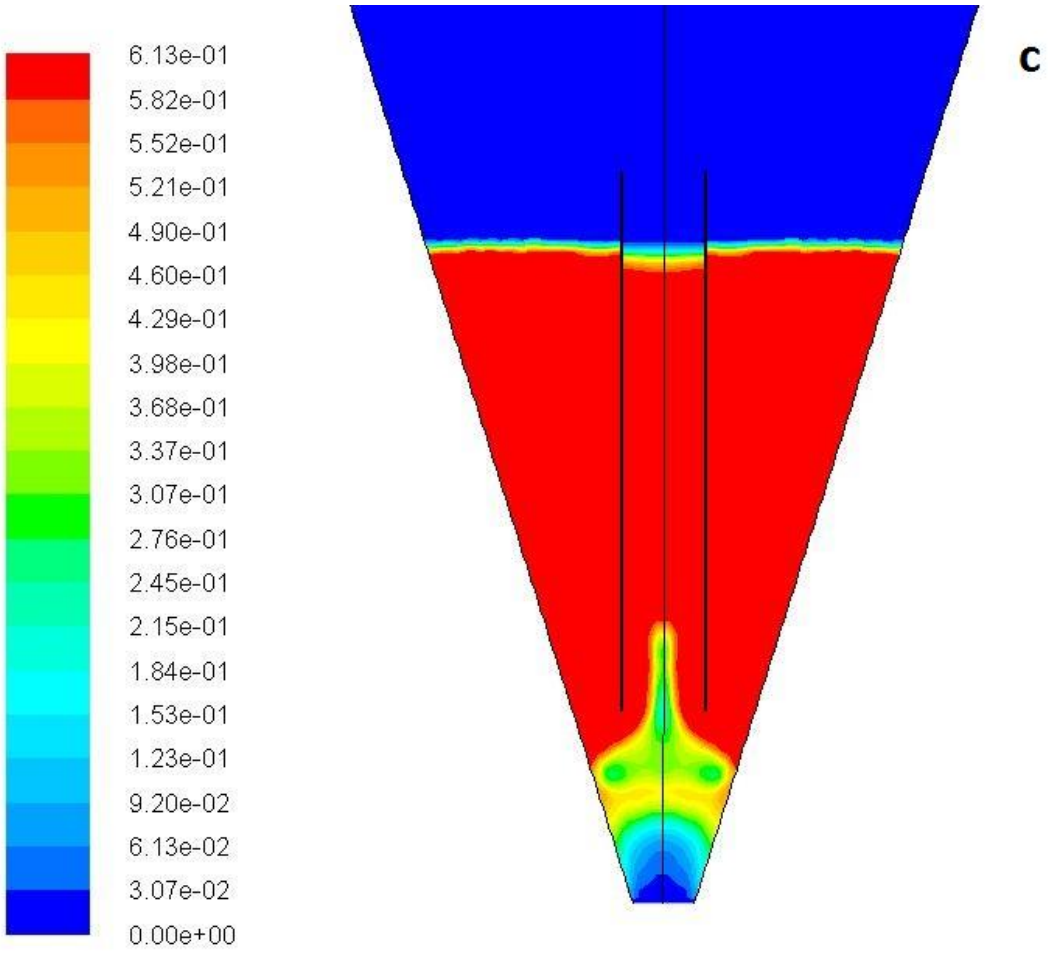
6.13e-01
5.82e-01
5.52e-01
5.21e-01
4.90e-01
4.60e-01
4.29e-01
3.98e-01
3.68e-01
3.37e-01
3.07e-01
2.76e-01
2.45e-01
2.15e-01
1.84e-01
1.53e-01
1.23e-01
9.20e-02
6.13e-02
3.07e-02
0.00e+00
C

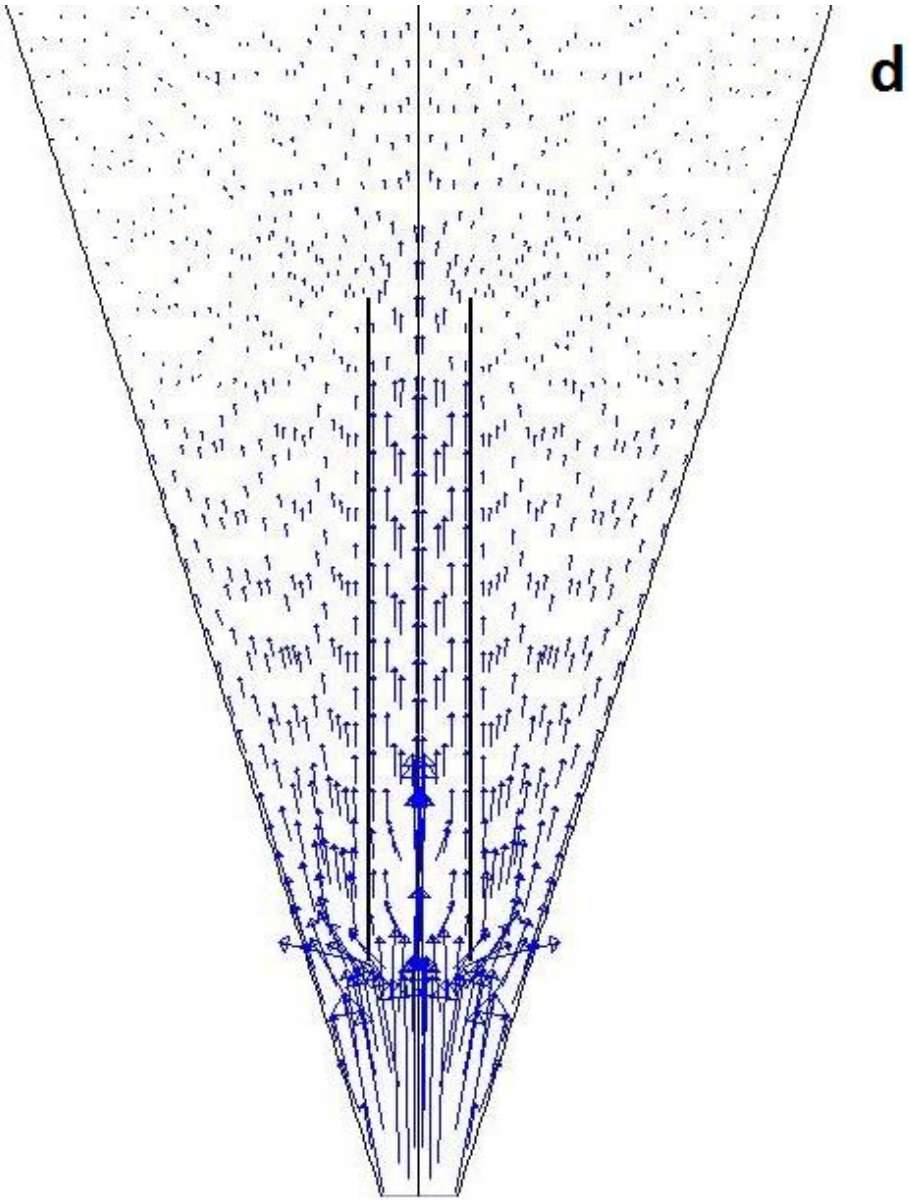

Fig. 9. Solid-phase contours and gas-phase velocity vectors at T=500 C and t=15 s; a) solid-phase volume fraction at L_H/D_T= 1.5, b) Nitrogen velocity vectors at L_H/D_T= 1.5, c) solid-phase volume fraction at L_H/D_T= 2.5, d) Nitrogen velocity vector at L_H/D_T= 2.5.

The impact of the draft tube on the bed stability and product formation has also been investigated. As can be observed in Fig. 10, not only the stable spouting cannot be reached,

but also the products do not form because of the poor mixing of particles in the bed; hence heat cannot transfer properly to the sand and biomass particles. The values of bio-oil and gas mass, in this case, were respectively 0.0035 and 1.0e-05 g, which deviated 94 and 98 percent from the original experimental values.

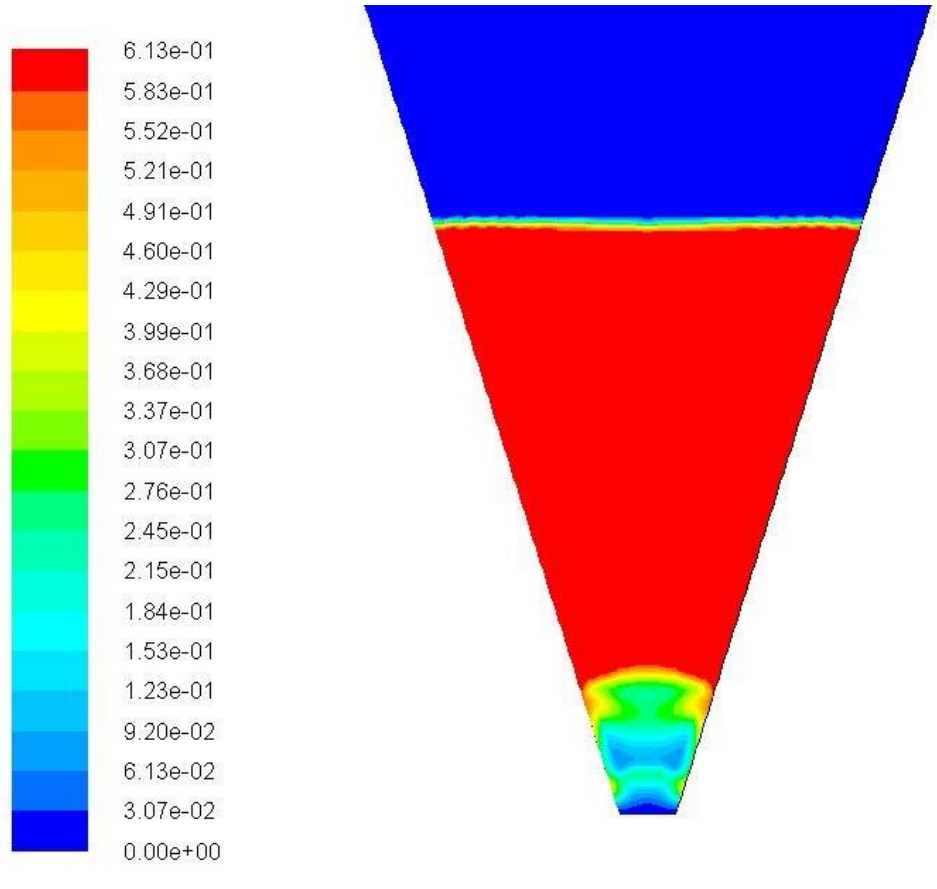

Fig 10. Solid-phase contours without the draft tube at t=15 s and T=500 °C.

5. Conclusions

A CFD model has been developed by combining a two-phase Eulerian approach and a kinetic model, which consists of three parallel reactions for the formation of the pyrolysis products (gas, bio-oil, and char) and a homogeneous secondary reaction in the gas phase (bio-oil cracking to yield gases). The simulation results were compared and validated with the

experimental data obtained at three different temperatures. The model was then used to predict the pyrolysis products in a lab-scale conical spouted bed reactor. The model showed a good agreement with experimental data in terms of both the hydrodynamic behavior of the bed and the final product yields and formation rates in biomass pyrolysis. As observed in our previous studies, the operating temperature has a significant impact on product yields. Accordingly, the CFD simulation model can be further applied in the design, optimization, and scale-up of conical spouted bed reactors for biomass fast pyrolysis processes.

Acknowledgments

This work was carried out with the financial supports from Iran's Ministry of Science, Research and Technology accompanied by Spain's ministries of Science, Innovation, and Universities (RTI2018-098283-J-I00 (MCIU/AEI/FEDER, UE)) and Science and Innovation PID2019-107357RB-I00 (MCI/AEI/FEDER, UE)), the European Union's Horizon 2020 research and innovation programme under the Marie Skłodowska-Curie grant agreement No. 823745, and the Basque Government (IT1218-19 and KK-2020/00107).

Nomenclature

C_D = Drag coefficient (-)

d_s: Particle diameter (m)

D_C, D_0, D_T: Diameter of the conical section, inlet and draft tube (cm)

e_{ss}: Restitution coefficient (-)

E: Activation energy (kJ mol^{-1})

g: Acceleration due to gravity (m s^{-2})

$g_{0,ss}$: radial distribution coefficient (-)

H_C, H_T : Height of the conical section and reactor (cm)

H_s, H_g: enthalpy of solid and gas (kJ mol^{-1})

h: Interphase heat transfer coefficient (-)

$\bar{\bar{I}}$: Stress tensor (-)

I_{2D}: Second invariant of the deviatoric stress tensor (-)

k_i, $k^0{}_i$: Kinetic constants at T temperature and frequency factor (s^{-1})

K_{gs}: gas/solid momentum exchange coefficient (Kg $m^{-3}s$)

L_H, L_T: Height of the entrainment zone and draft tube (cm)

Nu_s: Nusselt number (-)

Pr_s: Prandtel number (-)

P: Pressure (-)

P_s: solid-phase pressure (-)

R: Universal gas constant (-)

Re_s: Reynolds number (-)

Sq: Reaction source (Kg m^{-3} s^{-1})

T_i: Temperature (K)

v_i: Velocity (m s^{-1})

Y_i: Species mass fraction (-)

Greek letters

α_i: Volume fraction (-)

Θ_s: Granular temperature (m^2 s^{-2})

λ_s: Solid bulk viscosity (kg m^{-1} s^{-1})

μ_i: Shear viscosity (kg m^{-1} s^{-1})

ρ_i: Density (kg m^{-3})

$\bar{\bar{\tau}}_i$: Stress tensor (Pa)

ϕ: Angle of internal friction (deg)

Subscripts

fr: Friction

g: Gas

i: General index

p: Particle

q: Phase type (gas or solid)

s: solid

References

[1] Hydrogen council Hydrogen scaling up. A sustainable pathway for the global energy transition. 2017.

[2] Panwar NL, Kothari R, Tyagi VV Thermo chemical conversion of biomass – Eco friendly energy routes. Renewable and Sustainable Energy Reviews 2012;16:1801-16. doi:https://doi.org/10.1016/j.rser.2012.01.024.

[3] Kan T, Strezov V, Evans TJ Lignocellulosic biomass pyrolysis: A review of product properties and effects of pyrolysis parameters. Renewable and Sustainable Energy Reviews 2016;57:1126-40. doi:https://doi.org/10.1016/j.rser.2015.12.185.

[4] Xiong Q, Zhang J, Xu F, Wiggins G, Daw C. S. Coupling DAEM and CFD for simulating biomass fast pyrolysis in fluidized beds. J Anal Appl Pyrolysis 2016; 117: 176-181. https://doi.org/10.1016/j.jaap.2015.11.015

[5] Bridgwater A.V, Principles and practice of biomass fast pyrolysis processes for liquids, J. Anal. Appl. Pyrolysis 51 (1999) 3-22.

[6] Kabir G, Hameed BH Recent progress on catalytic pyrolysis of lignocellulosic biomass to high-grade bio-oil and bio-chemicals. Renewable and Sustainable Energy Reviews 2017;70:945-67. doi:https://doi.org/10.1016/j.rser.2016.12.001.

[7] Elliott DC, Hart TR, Neuenschwander GG, Rotness LJ, Zacher AH Catalytic hydroprocessing of biomass fast pyrolysis bio-oil to produce hydrocarbon products. Environ Prog Sustainable Energy 2009;28:441-9. doi:10.1002/ep.10384.

[8] Oasmaa A, Fonts I, Pelaez-Samaniego MR, Garcia-Perez ME, Garcia-Perez M Pyrolysis Oil Multiphase Behavior and Phase Stability: A Review. Energy Fuels 2016;30:6179-200. doi:10.1021/acs.energyfuels.6b01287.

[9] Lehto J., Oasmaa A., Solantausta Y., Kytö M., Chiaramonti D. Review of fuel oil quality and combustion of fast pyrolysis bio-oils from lignocellulosic biomass. Appl Energy 2014;116:178-90. doi:10.1016/j.apenergy.2013.11.040.

[10] Dabros TMH, Stummann MZ, Høj M, et al. Transportation fuels from biomass fast pyrolysis, catalytic hydrodeoxygenation, and catalytic fast hydropyrolysis. Prog Energy Combust Sci 2018;68:268-309. doi:10.1016/j.pecs.2018.05.002.

[11] Valle B, Remiro A, García-Gómez N, Gayubo AG, Bilbao J, Recent research progress on bio-oil conversion into bio-fuels and raw chemicals: a review. J Chem Technol Biotechnol 2019;94:670-89. https://doi.org/10.1002/jctb.5758.

[12] Mead DJ, Sustainable management of *Pinus radiata* plantations. FAO Forestry Paper. 2013; No. 170. Rome, FAO.

[13] Evans J, ed., Planted forests: uses, impacts and sustainability. 2009; Wallingford, United Kingdom, CABI and Rome, FAO.

[14] MMAMRM, Anuario de estadística forestal 2006. 2006; Madrid, Ministerio de Medio Ambiente y Medio Rural y Marino.

[15] Lopez G, Alvarez J, Amutio M, Hooshdaran B, Cortzar M, Haghshenasfard M, Hosseini SH, Olazar M, Kinetic modeling and experimental validation of biomass fast pyrolysis in a conical spouted bed reactor. Chem. En. J. 2019;373:677-86. https://doi.org/10.1016/j.cej.2019.05.072.

[16] Hameed S, Sharma A, Pareek V, Wu H, Yu Y, A review on biomass pyrolysis models: Kinetic, network and mechanistic models. Biomass Bioenerg. 2019;123:104-22. https://doi.org/10.1016/j.biombioe.2019.02.008.

[17] Wang S, Dai G, Yang H, Luo Z, Lignocellulosic biomass pyrolysis mechanism: A state-of-the-art review. Prog. Energy Combust. Sci. 2017;62:33-86. https://doi.org/10.1016/j.pecs.2017.05.004.

[18] SriBala G, Carstensen H-, Van Geem KM, Marin GB, Measuring biomass fast pyrolysis kinetics: State of the art. Wiley Interdiscip Rev. Energy Environ. 2019;8. https://doi.org/10.1002/wene.326.

[19] Makkawi Y, Yu X, Ocone R, Parametric analysis of biomass fast pyrolysis in a downer fluidized bed reactor. Renew. Energy 2019;143:1225-34. https://doi.org/10.1016/j.renene.2019.05.077.

[20] Xiong Q, Zhang J, Xu F, Ramirez E, Pannala S, Daw CS, Modeling the impact of bubbling bed hydrodynamics on tar yield and its fluctuations during biomass fast pyrolysis. Fuel, 2016; 164: 11-17. https://doi.org/10.1016/j.fuel.2015.09.074.

[21] Xiong Q, Xu F, Pan Y, Yang Y, Gao Zh, Shu Sh, Hong K, Bertrand F, Chaouki J, Major trends and roadblocks in CFD-aided process intensification of biomass pyrolysis. Chem. Eng. Process: Process Intensif. 2018;127:206-12. https://doi.org/10.1016/j.cep.2018.04.005.

[22] Eri Q, Wang B, Peng J, Zhao X, Li T, Detailed CFD modelling of fast pyrolysis of different biomass types in fluidized bed reactors. Can. J. Chem. Eng. 2018;96:2043-52. https://doi.org/10.1002/cjce.23180.

[23] Xiong Q, Yang Y, Xu F, Pan Y, Zhang J, Hong K, Lorenzini G, Wang Sh, Overview of Computational Fluid Dynamics Simulation of Reactor-Scale Biomass Pyrolysis. ACS Sustain. Chem. Eng. 2017;5:2783-98. https://doi.org/10.1021/acssuschemeng.6b02634.

[24] Papadikis K, Gerhauser H, Bridgwater AV, Gu S, CFD modelling of the fast pyrolysis of an in-flight cellulosic particle subjected to convective heat transfer. Biomass Bioenerg. 2009;33:97-107. https://doi.org/10.1016/j.biombioe.2008.04.021.

[25] Papadikis K, Gu S, Bridgwater AV, Gerhauser H, Application of CFD to model fast pyrolysis of biomass. Fuel Process Technol. 2009;90:504-12. https://doi.org/10.1016/j.fuproc.2009.01.010.

[26] Papadikis K, Gu S, Bridgwater AV, CFD modelling of the fast pyrolysis of biomass in fluidised bed reactors: Modelling the impact of biomass shrinkage. Chem. Eng. J. 2009;149:417-27. https://doi.org/10.1016/j.cej.2009.01.036.

[27] Papadikis K, Gu S, Bridgwater AV, 3D simulation of the effects of sphericity on char entrainment in fluidised beds. Fuel Process Technol. 2010;91:749-58. https://doi.org/10.1016/j.fuproc.2010.02.008.

[28] Papadikis K, Gu S, Bridgwater AV, Computational modelling of the impact of particle size to the heat transfer coefficient between biomass particles and a fluidised bed. Fuel Process Technol. 2010;91:68-79. https://doi.org/10.1016/j.fuproc.2009.08.016.

[29] Liu B, Papadikis K, Gu S, Fidalgo B, Longhurst PhJ, Li Zh, Kolios A, CFD modelling of particle shrinkage in a fluidized bed for biomass fast pyrolysis with quadrature method of moment. Fuel Process Technol. 2017;164:51-68. https://doi.org/10.1016/j.fuproc.2017.04.012.

[30] Boateng AA, Mtui PL, CFD modeling of space-time evolution of fast pyrolysis products in a bench-scale fluidized-bed reactor. Appl. Therm. Eng. 2012;33-34:190-8. https://doi.org/10.1016/j.applthermaleng.2011.09.034.

[31] Xue Q, Heindel TJ, Fox RO, A CFD model for biomass fast pyrolysis in fluidized-bed reactors. Chem. Eng. Sci. 2011;66:2440-52. https://doi.org/10.1016/j.ces.2011.03.010.

[32] Xue Q, Dalluge D, Heindel TJ, Fox RO, Brown RC, Experimental validation and CFD modeling study of biomass fast pyrolysis in fluidized-bed reactors. Fuel 2012;97:757-69. https://doi.org/10.1016/j.fuel.2012.02.065.

[33] Mellin P, Zhang Q, Kantarelis E, Yang W, An Euler-Euler approach to modeling biomass fast pyrolysis in fluidized-bed reactors - Focusing on the gas phase. Appl. Therm. Eng. 2013;58:344-53. https://doi.org/10.1016/j.applthermaleng.2013.04.054.

[34] Makibar J, Fernandez-Akarregi AR, Alava I, Cueva F, Lopez G, Olazar M, Investigations on heat transfer and hydrodynamics under pyrolysis conditions of a pilot-plant draft tube conical spouted bed reactor. Chem. Eng. Process: Process Intensif. 2011;50:790-8. https://doi.org/10.1016/j.cep.2011.05.013.

[35] Altzibar H, Lopez G, Bilbao J, Olazar M, Operating and peak pressure drops in conical spouted beds equipped with draft tubes of different configuration. Ind. Eng. Chem. Res. 2014;53:415-27. https://doi.org/10.1021/ie402031t.

[36] Makibar J, Fernandez-Akarregi AR, Diaz L, Lopez G, Olazar M, Pilot scale conical spouted bed pyrolysis reactor: Draft tube selection and hydrodynamic performance. Powder Technol. 2012;219:49-58. https://doi.org/10.1016/j.powtec.2011.12.008.

[37] Moliner C, Marchelli F, Bosio B, Arato E, Modelling of spouted and spout-fluid beds: Key for their successful scale up. Energies 2017;10:1729. https://doi.org/10.3390/en10111729.

[38] Lopez G, Alvarez J, Amutio M, Arregi A, Bilbao J, Olazar M, Assessment of steam gasification kinetics of the char from lignocellulosic biomass in a conical spouted bed reactor. Energy 2016;107:493-501. http://dx.doi.org/10.1016/j.energy.2016.04.040.

[39] Bellouard Q, Abanades S, Rodat S, Biomass Gasification in an Innovative Spouted-Bed Solar Reactor: Experimental Proof of Concept and Parametric Study. Energy Fuels 2017;31:10933-45. https://doi.org/10.1021/acs.energyfuels.7b01839.

[40] Elordi G, Olazar M, Lopez G, Amutio M, Artetxe M, Aguado R, Bilbao J, Catalytic pyrolysis of HDPE in continuous mode over zeolite catalysts in a conical spouted bed reactor. J. Anal. Appl. Pyrolysis 2009;85:345-51. https://doi.org/10.1016/j.jaap.2008.10.015.

[41] Lopez G, Olazar M, Amutio M, Aguado R, Bilbao J, Influence of tire formulation on the products of continuous pyrolysis in a conical spouted bed reactor. Energy Fuels 2009;23:5423-31. https://doi.org/10.1021/ef900582k.

[42] Rahimi-Ahar Zohreh, Hatamipour MS, Hydrodynamics, numerical study and application of spouted bed. Rev. Chem. Eng. 2018; 34:743-66. https://doi.org/10.1515/revce-2017-0036.

[43] Wang Z, Li H, Lim CJ, Grace JR, Oxidative torrefaction of spruce-pine-fir sawdust in a slot-rectangular spouted bed reactor. Energy Convers. Manage. 2018;174:276-87. https://doi.org/10.1016/j.enconman.2018.08.035.

[44] Kulah G, Sari S, Koksal M, Particle velocity, solids hold-up, and solids flux distributions in conical spouted beds operating with heavy particles. Ind. Eng. Chem. Res. 2016;55:3131-8. https://doi.org/10.1021/acs.iecr.5b04496.

[45] Arabiourrutia M, Lopez G, Elordi G, Olazar M, Aguado R, Bilbao J, Product distribution obtained in the pyrolysis of tyres in a conical spouted bed reactor. Chem. Eng. Sci. 2007;62:5271-5. https://doi.org/10.1016/j.ces.2006.12.026.

[46] Pietsch S, Peter A, Wahl P, Khinast J, Heinrich S, Measurement of granule layer thickness in a spouted bed coating process via optical coherence tomography. Powder Technol. 2019;356:139-47. https://doi.org/10.1016/j.powtec.2019.08.022.

[47] Brito RC, Béttega R, Freire JT, Energy analysis of intermittent drying in the spouted bed. Dry Technol. 2019;37:1498-510. https://doi.org/10.1080/07373937.2018.1512503.

[48] Zhong H, Xiong Q, Zhu Y, Liang S, Zhang J, Niu B, Zhang X, CFD modeling of the effects of particle shrinkage and intra-particle heat conduction on biomass fast pyrolysis. Renew. Energy 2019;141:236-45. https://doi.org/10.1016/j.renene.2019.04.006.

[49] Bao X, Du W, Xu J, An overview on the recent advances in computational fluid dynamics simulation of spouted beds. Can. J. Chem. Eng. 2013;91:1822-36. https://doi.org/10.1002/cjce.21917.

[50] Perkins G, Bhaskar T, Konarova M, Process development status of fast pyrolysis technologies for the manufacture of renewable transport fuels from biomass. Renew. Sustain. Energy Rev. 2018;90:292-315. https://doi.org/10.1016/j.rser.2018.03.048.

[51] Garcia-Nunez JA, Pelaez-Samaniego MR, Garcia-Perez ME, Fonts I, Abrego J, Westerhof RJM, Garcia-Perez M, Historical developments of pyrolysis reactors: A review. Energy Fuels 2017;31:5751-75. https://doi.org/10.1021/acs.energyfuels.7b00641.

[52] Liang X, Kozinski J, Numerical modeling of combustion and pyrolysis of cellulosic biomass in thermogravimetric systems. Fuel 2000; 79:1477-86. https://doi.org/10.1016/S0016-2361(99)00286-0.

[53] Lamarche P, Tazerout M, Gelix F, Köhler S, Mati K, Paviet F, Modelling of an indirectly heated fixed bed pyrolysis reactor of wood:

transition from batch to continuous staged gasification. Fuel 2013;106: 118-28. https://doi.org/10.1016/j.fuel.2012.12.005.

[54] Ghabi C, Benticha H, Sassi M, Two-dimensional computational modeling and simulation of wood particles pyrolysis in a fixed bed reactor. Combust. Sci. Technol. 2008;180:833-53. https://doi.org/10.1080/00102200801894091.

[55] Romagnosi L, Gascoin N, El-Tabach E, Fedioun I, Bouchez M, Steelant J, Pyrolysis in porous media: Part 1. numerical model and parametric study. Energy Convers. Manage. 2013;68:63-73. https://doi.org/10.1016/j.enconman.2012.12.023.

[56] Xiong Q, Kong S.-C, Passalacqua A, Development of a generalized numerical framework for simulating biomass fast pyrolysis in fluidized-bed reactors. Chem. Eng. Sci. 2013;99:305-13. https://doi.org/10.1016/j.ces.2013.06.017.

[57] Mellin P, Kantarelis E, Yang W, Computational fluid dynamics modeling of biomass fast pyrolysis in a fluidized bed reactor, using a comprehensive chemistry scheme. Fuel 2014;117:704-15. https://doi.org/10.1016/j.fuel.2013.09.009.

[58] Alvarez J, Amutio M, Lopez G, Barbarias I, Bilbao J, Olazar M, Sewage sludge valorization by flash pyrolysis in a conical spouted bed reactor. Chem. Eng. J. 2015;273:173-83. https://dx.doi.org/10.1016/j.cej.2015.03.047.

[59] Alvarez J, Lopez G, Amutio M, Artetxe M, Barbarias I, Arregi A, Bilbao J, Olazar M, Characterization of the bio-oil obtained by fast pyrolysis of sewage sludge in a conical spouted bed reactor. Fuel Process. Technol. 2016;149:169-75. https://doi.org/10.1016/j.fuproc.2016.04.015.

[60] Lopez G, Alvarez J, Amutio M, Mkhize NM, Danon B, Gryp P, Görgens JF, Bilbao J, Olazar M, Waste truck-tyre processing by flash pyrolysis in a conical spouted bed reactor. Energy Convers. Manage. 2017;142:523-32. https://doi.org/10.1016/j.enconman.2017.03.051.

[61] Cammarata L, Lettieri P, Micale GDM, Colman D, 2D and 3D CFD simulations of bubbling fluidized beds using eulerian-eulerian models. Int. J. Chem. Reactor. Eng. 2002;1. https://doi.org/10.2202/1542-6580.1083.

[62] Gidaspow D, Multiphase flow and fluidization: Continuum and kinetic theory descriptions, first ed. Academic Press, New York. 1994.

[63] Gidaspow D, Bezburuah R, Ding J, Hydrodynamics of circulating fluidized beds, Kinetic theory approach, fluidization VII. Proceedings of the seventh engineering foundation conference on fluidization, Gold Coast (Australia) 1992:75-82.

[64] Schaeffer DG, Instability in the evolution equations describing incompressible granular flow. J. Differ. Equ. 1987;66:19-50. https://doi.org/10.1016/0022-0396(87)90038-6.

[65] Gunn DJ, Transfer of heat or mass to particles in fixed and fluidised beds. Int. J. Heat Mass Transf. 1978;21:467-76. https://doi.org/10.1016/0017-9310(78)90080-7.

[66] Bridgwater AV, Review of fast pyrolysis of biomass and product upgrading, Biomass Bioenergy 2012;38:68-94. https://doi.org/10.1016/j.biombioe.2011.01.048.

[67] Altzibar H, Lopez G, Bilbao J, Olazar M, Minimum Spouting Velocity of Conical Spouted Beds Equipped with Draft Tubes of Different Configuration. Ind. Eng. Chem. Res. 2013;52:2995-3006. https://doi.org/10.1021/ie302407f.

[68] Mollick PK, Pandit AB, Vijayan PK, Parameters affecting efficient solid circulation rate in draft tube spouted bed. Ind. Eng. Chem. Res. 2018;57:8605-11. https://doi.org/10.1021/acs.iecr.8b01691.

[69] Ishikura T, Nagashima H, Ide M, Hydrodynamics of a spouted bed with a porous draft tube containing a small amount of finer particles. Powder Technol. 2003;131:56-65. https://doi.org/ 10.1016/S0032-5910(02)00321-2.

[70] Ye B, Lim C, Grace J, Hydrodynamics of Spouted and Spout Fluidized-Beds at High-Temperature. Can. J. Chem. Eng. 1992;70:840-7.

[71] Wu M, Guo Q, Liu L, Hydrodynamic performance of a spout-fluid bed with draft tube at different temperatures. Ind. Eng. Chem. Res. 2014;53:1999-2010. https://doi.org/10.1021/ie4034494.

[72] Estiati I, Altzibar H, Olazar M, Particle cycle times in draft tube conical spouted beds, Chem. Eng. Trans 2014;39: 1669-1674. https://doi.org/10.3303/CET1439279.

[73] Ji H, Tsutsumi A, Yoshida K, Solid circulation in a spouted bed with a draft tube, J. Chem. Eng. Jpn. 1998; 31: 842-45. https://doi.org/10.1252/jcej.31.842.

[74] Nagaraju VD, Sridhar BS, Hydrodynamics and heat transfer characteristics of draft tube spouted bed roasting of groundnuts (Arachis hypogeae), Int. J. Sci. Technol. Res. 2014; 3: 178-186.